Ground-state phase diagram of the ordered columnar phases of liquid-crystal materials

M. Hébert and A. Caillé
Centre de Recherche en Physique du Solide and Département de Physique, Université de Sherbrooke, Sherbrooke, Québec, Canada J1K 2R1
(Received 29 June 1995)

We present the derivation of a microscopic Hamiltonian for the angular degrees of freedom of the molecules in their low-temperature columnar helical phase (H phase). The ground-state phase diagrams, in the cases of homogeneous and nonhomogeneous helices, are investigated analytically and numerically. They feature a gradual unwinding of the helices as the intermolecular interchain coupling field is increased and the presence of a critical field above which only the uniform phase is stabilized. For the case of realistic nonhomogeneous helices, the transition to the uniform phase is accompanied by the presence of four points from which an infinite number of higher-order commensurate phases spring. In addition, an interesting reentrance of phases occurs at a constant value of one of the interaction parameters. This calculation sheds light on the H phase of hexa(hexylthio)triphenylene, as well as revealing the richness of the full phase diagram.

PACS number(s): 61.30.Cz, 61.30.Gd, 64.60.Cn, 64.70.Rh

I. INTRODUCTION

The columnar phases [1] of liquid-crystal materials, having a two-dimensional triangular lattice structure, combine the complexity and richness of in-plane geometrical frustration with a three-dimensional helicity pattern of intrinsically helical columns. In this class of systems, the material composed of hexa(hexylthio)triphenylene (HHTT) molecules of disklike shape having a stiff planar triphenylene core linked by thiol groups to six carbon alkyl chains imposes itself as the prototype.

To guide us in the formulation of a typical microscopic Hamiltonian for the columnar phases of liquid-crystal materials, we follow below with a review and an analysis of the available experimental results obtained for the HHTT columnar phases. The intent is not to proceed to a detailed understanding of the HHTT liquid-crystal phases, even though specific conclusions will be reached at the end of this article. This approach is made necessary since this is among the early trials to model columnar phases microscopically and with secondary modifications, the general Hamiltonian should be applicable to specific columnar materials.

Orientational and positional orderings in HHTT have received a lot of attention [2–5] recently. This material is characterized by the formation of columns inscribed in a two-dimensional triangular lattice. Early x-ray diffraction studies [2] of oriented strands drawn from bulk material of HHTT liquid crystal in the low-temperature columnar phase ($62\,^{\circ}\mathrm{C} < T < 70\,^{\circ}\mathrm{C}$) have lead to the conclusion of the presence of a three-dimensional ordering of the positions of the molecules with a superlattice reconstruction resulting from the displacement, parallel to the columnar axis, of one-third of the columns by half an intracolumnar lattice spacing. In Ref. [2] the authors reported that the displaced columns had only short-range helical order. However, in a subsequent study [3,4] using an optimized choice of the molecular parameters, they proposed long-range helical order for every column. The resulting two-dimensional helical pattern is also of period-three, perpendicular to the columnar axis, the displaced columns having opposite helicity to the undisplaced columns. The helical order along the columns is derived to be incommensurate with an intermolecular intracolumnar rotation angle α of 45.5° [3].

Subsequently, in Ref. [5], high-resolution bulk powder x-ray diffraction experiments were conducted on HHTT liquid crystals. The author concluded that for this bulk powder sample, the helical pitch is commensurate with the underlying lattice with an intermolecular rotation angle α of 45°. The molecules of the undisplaced columns were shown to have identical in-plane orientations in a plane perpendicular to the columnar axis, while the molecules belonging to the displaced columns were rotated by 60° with respect to the undisplaced molecules [3]. In addition, in Ref. [5], mixtures of triphenylenes were studied. The ordered helical columnar phase was shown to be stable over a wide temperature range for effective tail lengths between 5.65 and 6.10 carbon atoms.

The above experimental results point to a complex situation where the helical pitch of the columns depends on the experimental conditions, commensurate for a stress-free bulk material and weakly incommensurate for an elongated strand geometry. In addition, the presence of the ordered helices shows a strong dependence on the mixture of the triphenylenes, which, in turn, certainly has an influence over the intermolecular interaction parameters.

At this point, it is interesting to recall the recent result obtained by de Gennes and Prost [6]. Their conclusion was the absence of conventional long-range order along the columnar axis in the hexagonal columnar phase of liquid crystals. Indeed, assuming an effective elastic energy involving only positional degrees of freedom, where the columns can slide freely over each other, the average squared fluctuations of the positions in the colum-

nar direction diverge like the length of the sample in the thermodynamic limit. However, the interaction between HHTT molecules stacked in piles for the columnar liquid crystal depends on both the translational and orientational degrees of freedom of the molecules. In this context, the elastic energy of the system that controls the long-wavelength deformations would have contributions coming from both the strain tensor and a tensor involving the spatial derivatives of the angular field variables. As a result, for two neighboring columns that have developed a short-range helical orientational ordering and can still slide freely on each other on a macroscopic length scale, the coupling of positional and orientational degrees of freedom would generate higher-order terms that impose order in the positions of the molecules along the columnar axis, in the form of quasi-long-range order [7]. It is in the framework of this quasi-long-range order of the positions of the molecules that we proceed to the determination of the ground-state phase diagram, assuming that the molecules are periodically spaced along the columnar axis with one-third of the columns rigidly displaced in the columnar direction by half a lattice spacing. This lattice deformation produces a period-three superstructure perpendicular to the columnar axis and a partial release of the triangular frustration in the basal plane. A similar situation exists for some of the ABX_3 magnetic materials, such as $RbFeBr_3$ [8] and $RbVBr_3$ [9], with a subsequent splitting of the chiral multicritical point. As a result, only the orientational degrees of freedom then participate in the interaction between molecules that are otherwise considered to have their plane perpendicular to the columnar axis.

Before begining the study of the three-dimensional case, it is important to review the results obtained for the one-dimensional models. The study of the phase diagram at $T = 0$ of a one-dimensional chiral planar model in a local anisotropy field of p-fold rotational symmetry and constant amplitude along the columnar axis has been completed previously using analytical and effective potential methods [10,11]. In the case of the absence of self-consistency between columns, this calculation points to a very different behavior for the undisplaced and displaced columns. The most striking result is that for the displaced colunms the phase of period-eight is unstable to the effective local field of sixfold rotational symmetry of an infinitesimal value. Otherwise, for the undisplaced columns that are immersed in a local field of threefold symmetry, the period-eight helical structure is deformed by the constant amplitude field, but its period remains unchanged. These results point to a complex situation that can only be resolved by the study of a three-dimensional model. A three-dimensional $T = 0$ phase diagram for the ordered columnar phase using a proper interaction potential was obtained by Plumer *et al.* [12] under the assumption that the pitch of the helices does not change with the strength of the interaction parameters remaining equal to its value of $\alpha = 45°$ for HHTT. As will be seen later, most of the structure of the phase diagram is missed within this approximation, in particular the possibility of total unwinding of the helices to give a uniform state along the columnar axis.

In this paper the phase diagram at $T = 0$ is obtained for a period-three positional modulation in the plane perpendicular to the columnar axis and a pitch of the helices that is allowed to adjust to the strength of the intercolumnar potential. In Sec. II the Hamiltonian for orientational degrees of freedom of a molecule having an octupolar moment is rederived using a different approach. In Sec. III the phase diagram for incommensurate phases having an homogeneous helical configuration is obtained analytically, allowing for a uniform phase at high values of the intercolumnar interaction parameters. In Sec. IV, the phase diagram that allows for nonhomogeneous commensurate phases is presented. Finally, Sec. V discusses the results, compares them with the existing experimental situation, and arrives at a general conclusion.

II. DERIVATION OF THE HAMILTONIAN

As indicated in the Introduction, the ground-state phase diagram is derived under the assumption that only the orientational degrees of freedom are free to adjust to give lowest-energy configurations. The first step in deriving the Hamiltonian is to propose a proper description of the molecular entity occupying the lattice sites. Following Plumer *et al.* [12], we write the mass distribution of the HHTT molecule in a multipole expansion. Taking into account the D_3 point symmetry of the molecule and assuming for simplicity a reflection symmetry in the mid-molecular planes perpendicular to the columnar axis, the lowest-order nonzero term is an octupolar moment represented by a rank-three tensor Q_{klm} in two dimensions ($k, l,$ or $m = x$ or y). The results are

$$\begin{aligned} Q_{xxx} &= q\cos 3\theta_i, \\ Q_{xxy} &= -q\sin 3\theta_i, \\ Q_{xyy} &= q\sin 3\theta_i, \\ Q_{yyy} &= -q\cos 3\theta_i, \end{aligned} \tag{1}$$

where q is the magnitude of the octupolar moment of the HHTT molecule and θ_i is the angle between one of the branches of the HHTT molecule and the x axis. In Ref. [12], a model Hamiltonian was constructed to be invariant with respect to the hexagonal symmetry of the lattice. In this paper, we proceed in a different way [13] by constructing the most general invariants to lowest order using the components of the tensor Q_{klm} and components of the vector connecting the neighboring molecules on the lattice. The first term, bilinear in the components of Q_{klm}, for the interaction between sites i and j is

$$\sum_{k,l,m} Q_{klm}\ (i)Q_{mlk}(j) = 4q^2\cos 3(\theta_i - \theta_j). \tag{2}$$

The next term, also bilinear in the components of Q_{klm}, is

$$\sum_{i,j}\sum_{k,l,m}\sum_{n,p,q} Q_{klm}(i)\ Q_{npq}(j)\ x_q(i,j)\ x_p(i,j) \times x_n(i,j)\ x_m(i,j)\ x_l(i,j)\ x_k(i,j), \tag{3}$$

where $x_q(i,j)$ are the two Cartesian components of the vector connecting sites i and j. It is easily shown that for the components of the octupolar moment and for neighboring sites inscribed on a lattice whose projection on a plane perpendicular to the columnar axis has a triangular symmetry, the above expression (3) reduces to the term

$$q^2 \sum_{i,j} \cos 3(\theta_i + \theta_j). \tag{4}$$

The presence of this second-order term, which is not invariant under a global rotation of the system, is a result of the octupolar moment nature of the HHTT molecules and will be seen later to give a rich phase diagram structure.

The next-order nonzero term would have to be of fourth order in the components of Q_{klm} since third-order terms are not possible. Indeed, changing θ_i into $\theta_i + \pi$ for all sites (a change that should leave the interaction Hamiltonian invariant) changes Q_{klm} into $-Q_{klm}$, thus excluding third-order invariants.

As shown in Fig. 1, the displacement of one-third of the columns in the direction of the columnar axis by half a lattice spacing transforms the triangular lattice into a honeycomb lattice, the centers of the hexagons forming a triangular lattice rotated by 30° with respect to the original triangular lattice, their lattice sites being given by

$$\vec{\rho}_{nm} = n\vec{a}_1 + m\vec{a}_2. \tag{5}$$

The equilibrium positions of the molecules in the ground state are

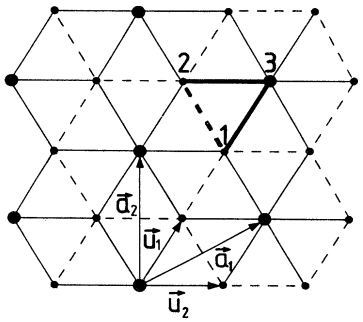

FIG. 1. Deformed lattice structure for a plane perpendicular to the columnar axis. The larger black dots represent displaced columns ($i = 3$) and the smaller dots the undisplaced columns ($i = 1$ and 2). The full lines are the J' and G' interactions and the dashed lines the J and G interactions. The triangle of heavy lines is the unit plaquette.

$$\vec{r}_{l_inm} = \left(l_i + \frac{1}{2}\delta_{i,3}\right)\hat{a}_z + \vec{\rho}_{nm} + \vec{u}_i, \tag{6}$$

where l_i specifies the coordinate in the columnar direction having $\hat{a}_z$ as a lattice vector, $i = 3$ stands for the displaced columns, and $i = 1$ or 2 represents the undisplaced columns. The basis vectors $\vec{u}_i$ are defined in Fig. 1. From the above, the bilinear first neighbor interaction Hamiltonian is written as

$$H = -\sum_{l_3,n,m}\sum_{l_t',n',m'}^{(12)} \left[J'\cos(\phi_{l_t'n'm'} - \phi_{l_3nm}) + G'\cos(\phi_{l_t'n'm'} + \phi_{l_3nm})\right]$$
$$-\frac{1}{2}\sum_{l_t,n,m}\sum_{l_t',n',m'}^{(3)} \left[J\cos(\phi_{l_t'n'm'} - \phi_{l_tnm}) + G\cos(\phi_{l_t'n'm'} + \phi_{l_tnm})\right] - \sum_{l_i,n,m}\cos(\phi_{l_i+1nm} - \phi_{l_inm} - \Delta), \tag{7}$$

where l_t stands for l_1 and l_2 and $\phi_{l_inm} = 3\theta_{l_inm}$. J' and G' are the interaction parameters between a site at the center of a hexagon and its 12 neighbors at the corners of the two hexagons below and above in the columnar direction. J and G are the interaction parameters between a site at the corner of a hexagon and its three neighbors at the corners of hexagons at the same level in the columnar direction. $\Delta = 3\alpha$, where α is the natural angle of rotation of two molecules superposed in the columns. All interaction parameters are measured in units of the first neighbor intracolumnar interaction parameter, which for simplicity is taken to be unity.

III. GROUND-STATE PHASE DIAGRAM FOR HOMOGENEOUS PHASES

It is easy to show [14] that the search for the ground states is reduced to a study of the ground states of a plaquette (shown in Fig. 1) of three columns with the interaction energy written as

$$E = -\sum_l \left[J\cos(\phi_{1l} - \phi_{2l}) + G\cos(\phi_{1l} + \phi_{2l})\right]$$
$$-\sum_l\sum_{i=1}^{2}\left[J'\cos(\phi_{3l} - \phi_{il}) + J'\cos(\phi_{3l} - \phi_{il+1})\right.$$
$$\left.+G'\cos(\phi_{3l} + \phi_{il}) + G'\cos(\phi_{3l} + \phi_{il+1})\right]$$
$$-\sum_l\sum_{i=1}^{3}\cos(\phi_{il+1} - \phi_{il} - \Delta). \tag{8}$$

In this section we limit the search to homogeneous phases with constant intracolumnar rotation angle Δ_i between neighboring molecules. We write

$$\phi_{il} = \phi_i + l\Delta_i C_i, \tag{9}$$

where $i = 1, 2,$ or 3. ϕ_i is the orientation of the molecule at level $l = 0$ in column i. Δ_i is the constant relative orientation of neighboring molecules in column i. C_i is ± 1 for right- or left-handed helicity accordingly. Under the assumption (9), the energy per site in the columnar direction reduces to

$$\begin{aligned}\epsilon = &-J\cos(\phi_1-\phi_2)\delta_{\Delta_1C_1-\Delta_2C_2,2\pi m} - G\cos(\phi_1+\phi_2)\delta_{\Delta_1C_1+\Delta_2C_2,2\pi m}\\ &-2J'\left[\cos\left(\frac{\Delta_2C_2}{2}\right)\cos\left(\phi_3-\phi_2-\frac{\Delta_2C_2}{2}\right)\delta_{\Delta_3C_3-\Delta_2C_2,2\pi m}\right.\\ &\left.+\cos\left(\frac{\Delta_1C_1}{2}\right)\cos\left(\phi_3-\phi_1-\frac{\Delta_1C_1}{2}\right)\delta_{\Delta_3C_3-\Delta_1C_1,2\pi m}\right]\\ &-2G'\left[\cos\left(\frac{\Delta_2C_2}{2}\right)\cos\left(\phi_3+\phi_2+\frac{\Delta_2C_2}{2}\right)\delta_{\Delta_3C_3+\Delta_2C_2,2\pi m}\right.\\ &\left.+\cos\left(\frac{\Delta_1C_1}{2}\right)\cos\left(\phi_3+\phi_1+\frac{\Delta_1C_1}{2}\right)\delta_{\Delta_3C_3+\Delta_1C_1,2\pi m}\right]-\sum_{i=1}^{3}\cos(\Delta_i-\Delta).\end{aligned} \tag{10}$$

δ is the Kronecker delta function and $m = 0$ or 1. In deriving the last term of (10) it has been assumed that the state of helicity Δ_i of column i is matched with the natural handedness of the stacking in that column.

As shown in [15], the difference between the unprimed and primed interaction parameters is certainly very small and for simplicity they will be taken to be equal, i.e., $J = J'$ and $G = G'$. An additional symmetry allows us to limit the study of the diagram to $G > 0$. Indeed, changing G into $-G$ only adds a constant angle $\pi/2$ to every angle ϕ_i, restoring the initial expression for the energy according to (10).

Initially, we present the general phase diagram obtained by numerical minimization of (10) for the different helicity patterns. Guided by the results exposed in Sec. I, we search only for the simple angular configurations where the three columns have identical intracolumnar rotational pitch $\Delta_1 = \Delta_2 = \Delta_3 = \Delta_0$. The commensurate states $\Delta_0 = 0$ and $\Delta_0 = \pi$ are also considered. Figure 2 presents the results for the phase diagram G versus J for $\Delta = \frac{3\pi}{4}$, which is the proper value of the natural pitch for HHTT [2,3].

As indicated, for $J > 0$, $J < G$, and small enough values of G for increasing J, the phase $(+++)_1$ is stable. From (10) it is easily shown that in this phase and under the conditions prescribed above, the rotational pitch changes continuously with J and is given by

$$\sin(\Delta - \Delta_0) = \frac{2}{3}J\sin\left(\frac{\Delta_0}{2}\right), \tag{11}$$

the relative angular pattern at level $l = 0$ being

$$\phi_2 = \phi_1, \tag{12a}$$

$$\phi_3 = \phi_1 + \frac{\Delta_0}{2}. \tag{12b}$$

For $J < 0$, $J < -G$, and small enough values of G for $|J| \to \infty$, the phase $(+++)_2$ is stable with the rotational pitch Δ_0 given by

$$\sin(\Delta - \Delta_0) = -\frac{J}{3}\sin(\Delta_0), \tag{13}$$

the relative angular pattern at level $l = 0$ being

$$\phi_2 = \phi_1 + \Delta_0, \tag{14a}$$

$$\phi_3 = \phi_1 + \Delta_0 + \pi. \tag{14b}$$

In both cases above, ϕ_1 is free and contributes to the infinite degeneracy of the ground state $(+++)_1$ and $(+++)_2$. The above two phases could have been labeled

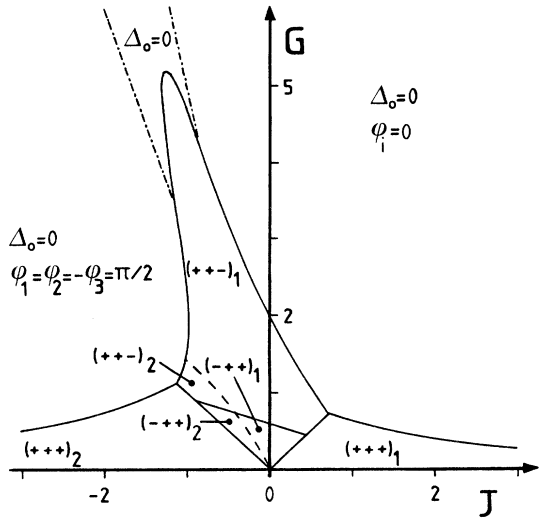

FIG. 2. Phase diagram for the uniform phases. The labels $(+++)_i$, $(++-)_i$, and $(-++)_i$ refer to the helicity pattern for the unit plaquette (1, 2, and 3, respectively). The subscript $i = 1$ or 2 is defined in the text. The full curves are boundaries between phases having a different Δ_0. The dash-dotted lines at $G = -5J$ and $-3J$ are second-order transition lines between uniform phases $\Delta_0 = 0$. The dashed lines inside phases $(++-)$ and $(-++)$ are separation lines as defined in the text.

$(---)_1$ and $(---)_2$.

Above the phase $(+++)_1$, for $J > 0$, and large enough values of G, it was found that the commensurate uniform phase $\Delta_0 = 0$ with $\phi_1 = \phi_2 = \phi_3 = 0$ is the stable ground state. The phase boundary between the phases $(+++)_1$ and $\Delta_0 = 0$ for $J \gg 1$ is given by

$$G \cong \frac{9}{10J} \sin^2 \Delta. \tag{15}$$

The uniform phase $\Delta_0 = 0$ has no helicity pattern and all the orientational degrees of freedom are totally frozen with $\phi_i = 0$ as a result of umklapp terms present in this case. Similarly, for $J < 0$ and $|J| \gg 1$, the phase boundary between the phase $(+++)_2$ and the phase $\Delta_0 = 0$ is given by

$$G \cong \frac{3}{2|J|} \sin^2 \Delta. \tag{16}$$

In this last case the angular coordinates are frozen to $\phi_1 = \phi_2 = -\phi_3 = \frac{\pi}{2}$.

The rest of the phase diagram, occupied by helically ordered phases, is shown in Fig. 2. The phase $(++-)$ appears in two forms. For $G \cos \frac{\Delta_0}{2} > -J$, phase $(++-)_1$ is stable with its rotational pitch Δ_0 given by

$$\sin(\Delta - \Delta_0) = \frac{2G}{3} \sin \frac{\Delta_0}{2} \tag{17}$$

and its relative angular pattern at level $l = 0$ being

$$\phi_2 = \phi_1, \tag{18a}$$

$$\phi_3 = -\phi_1 - \frac{\Delta_0}{2}. \tag{18b}$$

Again, the undetermined value of ϕ_1 allows for the infinite degeneracy of the ground state of $(++-)_1$. For $G = J$, the phase $(++-)_1$ is in equilibrium with the phase $(+++)_1$ with equal value of Δ_0. For $G \cos \frac{\Delta_0}{2} < -J$, the phase $(++-)_2$ is stable with its rotational pitch Δ_0 given by

$$\sin(\Delta - \Delta_0) = -\frac{G^2}{3J} \sin \Delta_0 \tag{19}$$

and its relative angular pattern at level $l = 0$ being

$$\phi_2 = \phi_1 + 2\cos^{-1}\left(-\frac{G}{J}\cos\frac{\Delta_0}{2}\right), \tag{20a}$$

$$\phi_3 = -\phi_1 - \frac{\Delta_0}{2} - \cos^{-1}\left(-\frac{G}{J}\cos\frac{\Delta_0}{2}\right). \tag{20b}$$

A separation line indicating the boundary between the two $(++-)$ phases is shown in Fig. 2. For $G = -J$, the phase $(++-)_2$ is in equilibrium with $(+++)_2$ having equal Δ_0. The phase $(++-)_1$ is bordered on the right-hand side by the uniform phase $\Delta_0 = 0$ with $\phi_i = 0$ and on the left-hand side by the uniform phase $\Delta_0 = 0$ with $\phi_1 = \phi_2 = -\phi_3 = \frac{\pi}{2}$. At larger values of G (as shown in Fig. 2), the phase $(++-)_1$ is limited to a narrow region bounded above by that part of the uniform phase $\Delta_0 = 0$ which makes the transition from the two uniform phases $\Delta_0 = 0$ existing, respectively, for $J \to \infty$ and $J \to -\infty$.

The phase $(-++)$ occupies a small fraction of the phase diagram near the origin above $G = \pm J$ (Fig. 2). For $G > -J(1 + 2\cos\frac{\Delta_0}{2})$, the phase $(-++)_1$ is stable with its rotational pitch Δ_0 given by

$$\sin(\Delta - \Delta_0) = \left(\frac{J+G}{3}\right) \sin\frac{\Delta_0}{2}, \tag{21}$$

its angular pattern at level $l = 0$ being

$$\phi_2 = -\phi_1, \tag{22a}$$

$$\phi_3 = -\phi_1 + \frac{\Delta_0}{2}. \tag{22b}$$

For $G = J$, the phase $(-++)_1$ is in equilibrium with $(+++)_1$ with the same value of Δ_0. For $G < -J(1 + 2\cos\frac{\Delta_0}{2})$, the phase $(-++)_2$ is stable, but no simple analytical expression was obtained for Δ_0 nor the angular pattern at $l = 0$. Again a separation line is shown in Fig. 2. For $G = -J$, the phase $(-++)_2$ is in equilibrium with the phase $(+++)_2$, with the same value of Δ_0 as the last.

On the boundary $G = J$, there is a point where the three phases $(+++)_1$, $(++-)_1$, and $(-++)_1$ are in equilibrium with the same value of Δ_0. Across the boundary between $(++-)_1$ and $(-++)_1$, Δ_0 changes in a discontinuous manner. It may be easily shown, using the expressions for the ground-state energies in phases $(++-)_1$ and $(-++)_1$, that the above-mentioned point on the $G = J$ line is given by

$$\cos\frac{\Delta_0^*}{2} = \frac{1}{2}, \tag{23}$$

i.e., $\Delta_0^* = \frac{2\pi}{3}$. Substituting in (11), (17), or (21), the triple point is given by $G_1^* = J_1^* = 0.4482...$, which is verified numerically in Fig. 2. The triple point between the phases $(+++)_2$, $(++-)_2$, and $(-++)_2$, for $G > 0$ and $J < 0$, is also given by $\Delta_0^* = \frac{2\pi}{3}$, which, from (13) or (19), gives the location $G_2^* = -J_2^* = 0.8965...$, again verified numerically in Fig. 2. Figure 3 shows a closeup of the local structure for the pinching of the separation lines in phases $(++-)$ and $(-++)$ with the phase boundary between phases $(++-)$ and $(-++)$. It clearly reveals two separate pinching points and a common boundary between $(++-)_1$ and $(-++)_2$.

As shown in Fig. 2, an intermediate uniform phase $\Delta_0 = 0$ separates the two uniform phases $\Delta_0 = 0$ existing at large values of G for $J \to \pm\infty$. We now show that the two straight lines may be obtained from a spin-wave instability mechanism. Indeed, approaching the boundary from the positive J where $\phi_1^0 = \phi_2^0 = \phi_3^0 = 0$, assuming by symmetry that $\phi_1 = \phi_2$ and fixing ϕ_3 to minimize the energy, we get the power expansion for the energy

$$\epsilon = \epsilon_0 + \left[4G + 2J - \frac{2(J-G)^2}{(J+G)^2}\right]\phi_1^2 + \left[-\frac{5G}{6} - \frac{J}{6} + \frac{1}{2}\frac{(J-G)^4}{(J+G)^3} - \frac{1}{3}\frac{(J-G)^2}{(J+G)}\right]\phi_1^4 + \cdots \tag{24}$$

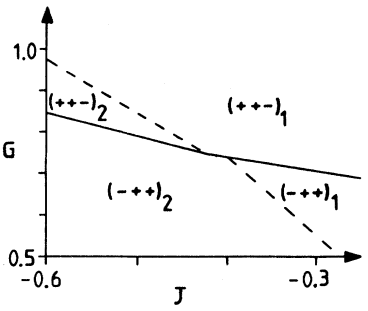

FIG. 3. Closeup of the pinching of the separation lines (dashed lines) with phase boundary between (+ + −) and (− + +) (full curve).

with $\phi_3 = \left(\frac{J-G}{J+G}\right)\phi_1$. The coefficient of ϕ_1^2 changes sign for $G = -5J$, while the coefficient of ϕ_1^4 remains positive. As shown in Fig. 2, this is indeed found numerically. Near the phase boundary inside the intermediate phase, the angular pattern at level $l = 0$ is given by

$$\phi_2 = \phi_1, \tag{25a}$$

$$\phi_3 \simeq -\frac{3}{2}\phi_1. \tag{25b}$$

For $G < -5J$, the value of ϕ_1 is fixed by the minimum of ϵ.

A similar argument, starting from the negative J, gives a phase boundary at $G = -3J$ and an angular pattern, near the phase boundary, inside the intermediate phase given by

$$\phi_2 = \phi_1 = \frac{\pi}{2} - \phi, \tag{26a}$$

$$\phi_3 = -\frac{\pi}{2} + \frac{\phi}{2}, \tag{26b}$$

where ϕ minimizes the energy. Hence the two straight lines are second-order transition lines, which terminate on the first-order transition boundary of the phase (+ + −).

In this section, by imposing homogeneous phases and not allowing for the distortions that would pin down the helical structures to the underlying lattice, the commensurate phases, with the exception of the uniform phase $\Delta_0 = 0$, occupy a region of measure zero in the phase diagram. In the next section, solving numerically for finite systems and allowing for distorting pinning effects, the commensurate phases are shown to occupy at least a large fraction, if not all, of the phase diagram, the general structure being maintained.

IV. NONHOMOGENEOUS MODULATED PHASES

In this section we study the occurrence of a nonhomogeneous phases in the ground-state phase diagram. This is done by relaxing the constraint that forces the angle between adjacent molecules in a column to be Δ_0. Each molecule now has complete rotational freedom, which is fixed to minimize the energy. As indicated above, this will stabilize commensurate phases over a finite domain in the parameter space.

In the case of homogeneous phases, the state of a column is described by its uniform pitch Δ_0 and the phase angle ϕ_i in a reference plane. For nonhomogeneous phases, it is described by the rotation angle of each molecule inside the column. The interaction energy between molecules on a triangular lattice (8) will enable us to treat the coupling between the columns exactly. In order to solve this problem, one has to perform a numerical simulation on a finite-size lattice. We took a system composed of three columns of $N_{\max}$ molecules ($N_{\max} = 32$), with periodic boundary conditions in all spatial directions. Due to the numerical limitations (finite-size lattice), the higher-order commensurate (period greater than $N_{\max}$) and incommensurate phases are not found. We argue that larger values of $N_{\max}$ would only refine the phase diagram without changing its main features and main boundaries. There are several methods that have been used to find the ground-state phase diagram [16,17] of similar systems. We adopt a method used to find starting configurations for Monte Carlo simulations [18]. This method was chosen because of its simplicity and straightforward applicability to complex tridimensional helical systems. For a specific set of parameters (J, G, and $\Delta = \frac{3\pi}{4}$), an initial angular configuration of the $3N_{\max}$ molecules ($N_{\max} = 32$) is selected. Two kinds of initial configurations were used. First, N_{ran} (typically $N_{\text{ran}} = 25$) configurations were generated by choosing the $3N_{\max}$ angular variables in a completely random fashion. Second, N_Δ (typically $N_\Delta = 5$) configurations were chosen as homogeneous helical patterns specified by (9) with a random phase angle ϕ_i for each column. The search for the commensurate phases of specific period in a system having global periodic boundary conditions of $3N_{\max}$ molecules was approached by considering systems of finite physical size of $3N_t$ molecules (with $N_t \leq N_{\max}$). For each site of the system, the field created locally by the neighboring molecules is calculated and the energy is minimized by aligning the molecule in its local anisotropy field. This iterative process was continued until self-consistency was reached. Convergence to the true ground state was not achieved for every initial angular configuration and we used the criteria of lowest energy to select among those. Every physical size of the system ($3N_t$ molecules with $1 \leq N_t \leq N_{\max}$) was then checked in this manner to find the selected ground-state configuration.

This technique allows the pinning, by umklapp terms, of commensurate phases over a wide portion of the phase diagram. It also gives fan structures, typical of such systems, clearly visible in Fig. 4. These structures were not possible for the case of a homogeneous phase (no umklapp terms except for the uniform phase 0/1). To identify the commensurate phases, we introduce the generalized winding number [17] of the column i

$$\omega_i = \frac{1}{q_i}\sum_{n=1}^{q_i}\Theta(k_i(\phi_{i,n-1} - \phi_{i,n})) = \frac{p_i}{q_i}, \tag{27}$$

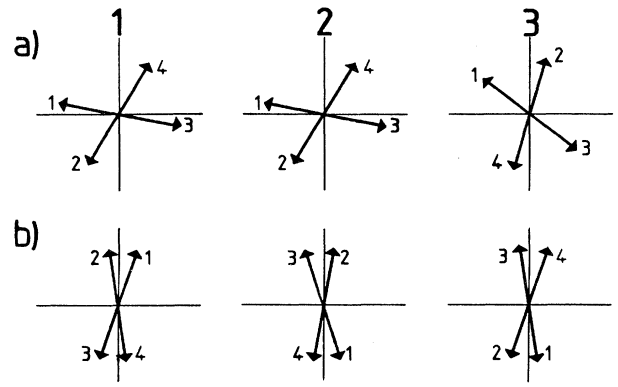

FIG. 4. Typical angular configurations in a particular phase ($\omega = \frac{1}{4}$). Large numbers identify the columns and small numbers identify the particular molecules in a column for (a) $J = -0.5$ and $G = 1.5$ and (b) $J = -1.0$ and $G = 1.5$.

where q_i is the period of the angular configuration, k_i is the helicity of the column, and Θ is the Heaviside step function. For example, the structures in Fig. 4 clearly have the same winding number $\omega = \frac{1}{4}$.

In Figs. 5 and 6 we present the global and closeup phase diagrams obtained using the technique described above. The first observation is that the winding numbers of the three columns are found to be the same for the parameter range studied. Second, it is found that the general features of the phase diagram of the homogeneous modulated phases are maintained. The uniform 0/1 phase occupies a large fraction of the parameter space. Its phase boundary with other phases have the same elongated structure along the abscissa and the same tilted form along the $G \simeq -4J$ line. The helicity configurations for the $(+\,+\,+)$ and $(+\,+\,-)$ cases are again separated by the $G = \pm J$ lines, a result consistent with the results obtained earlier [15].

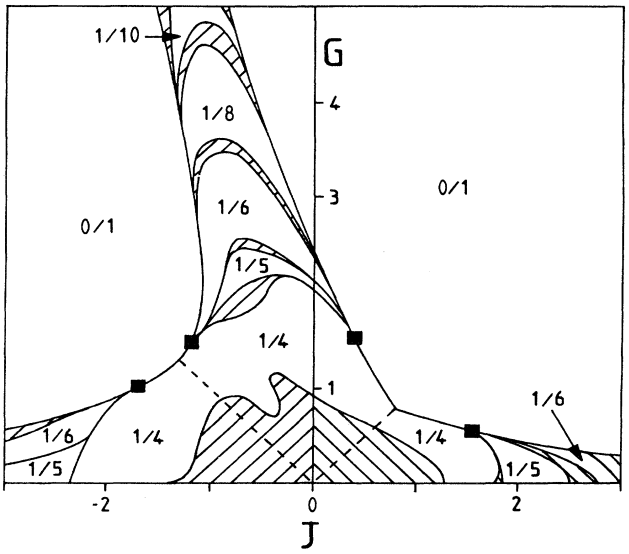

FIG. 5. Global ground-state phase diagram of Eq. (8) as a function of J and G. Each phase is noted by its winding number ω. The helicity configuration is $(+\,+\,+)$ below the dashed lines $G = \pm J$ and $(+\,+\,-)$ over the same dashed lines; regions between identified phases are higher-order commensurate or incommensurate phases. The hatched region near the origin is presented in Fig. 6. The four full squares represent Υ points as defined in the text.

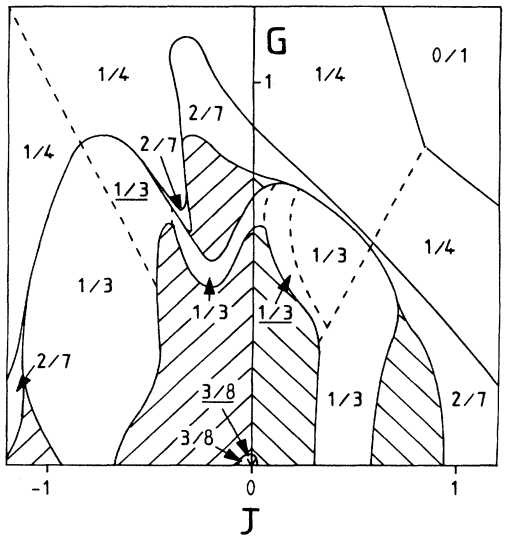

FIG. 6. Closeup ground-state phase diagram of Eq. (8) as a function of J and G. The phases and helicity configurations are denoted as in Fig. 5, with the exception that underlined winding numbers refer to the $(-\,+\,+)$ helicity configuration. Again, the dashed lines separate $(+\,+\,+)$ from $(-\,+\,+)$ and $(+\,+\,-)$ helicity patterns.

As seen in Fig. 5, a set of simple commensurate phases of winding number smaller than 1/4 occupy the inside of the elongated portion of the phase diagram along the abscissa and the $G \simeq -4J$ line. The domain of stability of each of these commensurate phases emerges with an infinitesimal width from four points in parameter space (Υ points) that are denoted by squares in Fig. 5. The locations of these points have been determined numerically by the method described earlier and are given by

$$\begin{aligned}(J_\Upsilon, G_\Upsilon) &= (0.425, 1.55)\\ &= (1.54, 0.557)\\ &= (-1.22, 1.44)\\ &= (-1.70, 1.02).\end{aligned} \tag{28}$$

Each of these points is situated at the end of a common boundary between the uniform 0/1 phase and the 1/4 phase. Exactly at an Υ point, the phases with winding number $\omega \leq 1/4$ and the uniform 0/1 phase have the same energy. On one side of an Υ point, the system goes directely from the 1/4 to the 0/1 phase via a first-order transition. On the other side, this transition is not direct; a complete devil's staircase (starting with the winding number $\omega = 1/4$) is found. As one moves away from the Υ point on this side, each phase with $\omega < 1/4$

is stabilized over a finite portion of the parameter space.

To understand the transition mechanism near an Υ point, we analyzed the first point in (28). Near this point, the numerical procedure described above can give us the lowest-energy angular configuration for a given pitch (we considered the phases with pitch $1/q$ with $q \geq 4$). Those configurations are represented in Fig. 7. They were used with (8) to calculate the ground-state energy by minimizing with respect to θ and ϕ. The location of the Υ point found with this technique is consistent with (28). This technique also confirms that, for $J > J_\Upsilon$, the system goes directly from the 1/4 phase to the uniform 0/1, while for $J < J_\Upsilon$, a cascade of phases is stabilized over a finite region between the 1/4 and 0/1 phases. The observation of Fig. 7 also gives a hint about the transition mechanism from the phases 1/4 to 0/1. In going to higher-order commensurate phases $[1/(6+m)$ with $m \geq 1]$, each additional molecule is placed at $\phi_i = 0$. This mechanism gives a gradual unwinding of the columns until $m \to \infty$ for the uniform 0/1 phase.

For the choice of physical parameter ($\Delta = \frac{3\pi}{4}$), the phase with winding number 1/4 forms a simply connected region touching both positive and negative values of J.

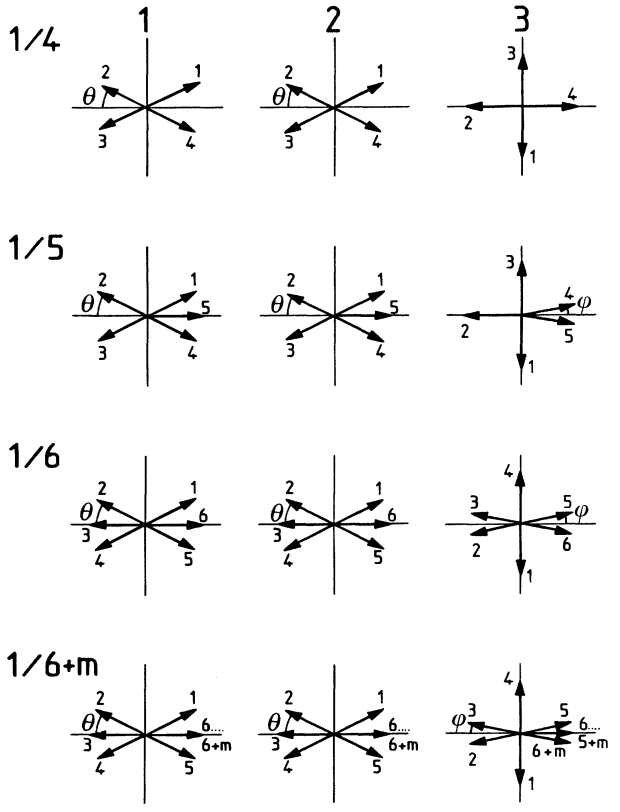

FIG. 7. Lowest-energy angular configuration, for a given pitch $1/q$ with $q \geq 4$, near the Υ point situated at (J_Υ, G_Υ) = (0.425,1.55). Large (small) numbers represent columns (molecules). In going to higher-order commensurate phases $[1/(6+m)$ with $m \geq 1]$, each additional molecule is placed at $\phi_i = 0$.

The Υ points (28) are also the loci of convergence of the domain of stability of the higher-order commensurate phases springing from the $G = 0$ axis for positve and negative J.

The higher-order commensurate phases ($q > 4$) existing inside the elongated portion centered on the $G \simeq -4J$ line show an interesting reentrance of phases. Indeed, for a constant value of G, there exist two regions of J where the phases $1/q$ ($q > 4$) are stable. One of these regions is entirely located on the negative side of the J axis. This reentrance behavior is a reminescence of the existence of two distinct uniform phases 0/1 in the limits of $J \to \pm\infty$. The first step in the understanding of the phenomena is to recall that the interactions are dominated by terms involving displaced molecules (belonging to columns 1 and 2), since there are 12 nearest neighbors in this case compared to 3 for the terms between undisplaced molecules. Neglecting the modulation, for positive value of G, the dominant terms assume their maximum negative values for $\phi_1 = \phi_2 = \phi_3 = 0$ or $\phi_1 = \phi_2 = -\phi_3 = \pi/2$. Changing the value of J (from positive to negative) drives the system from configurations close to the first extremum condition ($\phi_1 = \phi_2 = \phi_3 = 0$) to finally a set of configurations close to the second condition ($\phi_1 = \phi_2 = -\phi_3 = \pi/2$). The existence of these two distinct sets of configurations explains the reentrance of a second domain of stability for the $1/q$ phase with decreasing value of J.

Figure 6 shows a closeup of some of the phases appearing near the origin, below the simply connected region occupied by the 1/4 phase mentioned above. For $G \ll 1$ and $J \ll 1$, the 3/8 phase has a finite domain of stability. It is to be noted that, depending on the choice of interaction parameters, the two helicity patterns predicted for homogeneous phases are observed. Indeed, for $G < |J|$ the helicity pattern $(+++)$ is seen and for $G > |J|$ the

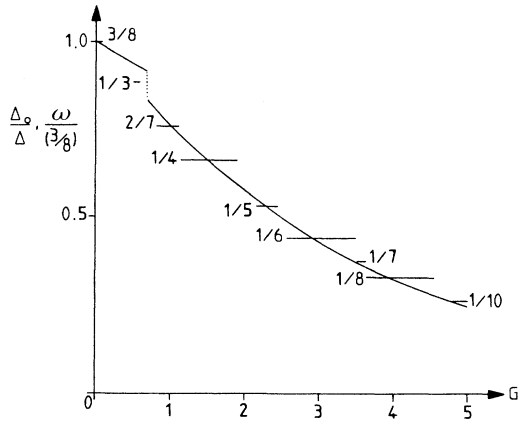

FIG. 8. Pitch of helices for the homogeneous modulated phases (Δ_0/Δ, where $\Delta = \frac{3\pi}{4}$) (solid curve) and winding number for the nonhomogeneous modulated phases ($\omega/\frac{3}{8}$) (horizontal lines) against G along the $G = -4J$ line. The helicity configuration transition between the $(-++)$ and $(++-)$ patterns occurs at $G \simeq \frac{2}{3}$ for the homogeneous phases, while the transition in the nonhomogeneous modulated phases happens somewhere between the 3/8 and 1/3 phases.

helicity pattern $(- + +)$ is predicted. There is another region of the 3/8 phase observed inside the limit seen in Fig. 6. However, it is rejected as being an artifact of the finite-size lattice since its domain of stability is shown to decrease enormously with increasing size (e.g., $N_{\max} = 50$). Further away from the origin, the 1/3 phase is shown to occupy a fully connected region starting at $J > 0$ and ending at $J < 0$. For $G > |J|$, regions of helicity $(+ + -)$ and $(- + +)$ are shown to exist. This 1/3 phase is bordered on its outside by a 2/7 phase, which occupies also a fully connected region as far as can be determined with finite-size calculations.

Figure 8 shows the variation of the relative pitch Δ_0/Δ for homogeneous phases as a function of G on the $G = -4J$ line. The jump near $G = 0.666$ appears when going from the helicity pattern $(- + +)$ to the helicity pattern $(+ + -)$. Otherwise, the curve is continuous and given by (17) in the helicity pattern $(+ + -)$. On the same figure, we have added the horizontal plateaus for the winding number $\omega/\frac{3}{8}$ with their finite width as a function of G for these nonhomogeneous phases.

V. DISCUSSION AND CONCLUSION

For both the homogeneous and nonhomogeneous three-dimensional commensurate phases, we have presented above the effect of self-consistent intercolumnar intermolecular interactions. Indeed, globally, they reduce the average intracolumnar intermolecular relative angular orientation from its value in the absence of intercolumnar interactions, leading to a progressive unwinding of the helices with increasing values of the intermolecular interaction parameters. The above results from treating the field acting on a given column self-consistently with the global angular configuration of the columns. The general behavior may be extracted from single column calculations. As indicated in the Introduction, single column calculations in a non-self-consistent field were performed before and lead to results whose comparison with the above is interesting. Two features of the phase diagrams (Figs. 2 and 5) can be explained by treating the intercolumnar coupling as an on-site field having the symmetry of the environment experienced by each molecule. The first feature is the existence of a critical field above which the only phase stabilized is the uniform phase. The second is the gradual unwinding of the helices as J or G increases, reported explicitly in Fig. 8.

As seen from the positions of the molecules in the two-dimensional network, the displaced columns are subject to a sixfold anisotropy field, while the undisplaced ones are subject to a threefold anisotropy field (see Fig. 1). Within a non-self-consistent approximation, the intensity of the equivalent crystal field can be roughly taken as proportional to J and G. Since the HHTT molecules have threefold internal rotational symmetry, one can map those systems of columns on one-dimensional chiral planar spin models in a $\frac{p}{3}$-fold anisotropy field with $p = 6$ or 3, respectively. The ground-state phase diagram of a chiral planar model in a twofold anisotropy field (easy-axis field) has been reported by Hébert *et al.* [10]. They concluded to a gradual winding of the helix as the field is increased for $\frac{\pi}{2} \leq \Delta \leq \pi$ and to the existence of a multiphase point at infinite field. In contrast to this, the ground-state phase diagram of a chiral planar model in a onefold anisotropy field (equivalent to a magnetic field), as investigated by Yokoi *et al.* [19], shows the unwinding of the helix as the field is increased for $0 \leq \Delta \leq \pi$ and the presence of a critical field above which only the ferromagnetic phase is stabilized.

The presence of two undisplaced columns (threefold anisotropy field) for each displaced column (sixfold anisotropy field) and the fact that displaced columns only interact through the undisplaced columns when interactions are limited to first neighbor interactions, thus are enough to force the whole system to unwind with a unique periodicity for all columns. Along the $G = -4J$ line in Fig. 8, this unwinding of the helical phases is halted at a finite value of G, where the uniform phase becomes energetically favorable as exists when the dominant undisplaced columns are treated individually [10].

As indicated before, the orientational ordering of the angular degrees of freedom for the triangular columnar phase of liquid crystals such as HHTT should have a lot in common with the antiferromagnetically frustrated triangular structure of some ABX_3 compounds [20]. Like in some ABX_3 compounds [8,9], the triangular frustration is partially lifted in the ground state of the columnar liquid crystal as a result of a superlattice deformation displacing one-third of the columns in the direction of the columnar axis. In addition to this partially lifted frustration, for the liquid-crystal material such as HHTT, it was shown in Sec. II that a nonrotationally invariant term appears to second order in the intercolumnar potential energy. As shown in Secs. III and IV, this addition brings about quite a number of different features in the ground-state phase diagram.

Let us first consider the situation with $G = 0$. For positive values of J, an ordered phase with fully parallel orientation is achieved, as shown by Eqs. (12a) and (12b), additional $\Delta_0/2$ for column 3 resulting from the displacement by half a lattice spacing in the c direction. For $J < 0$, the ground-state angular configuration when redrawn in the $l = 0$ plane is as given in Fig. 9(a).

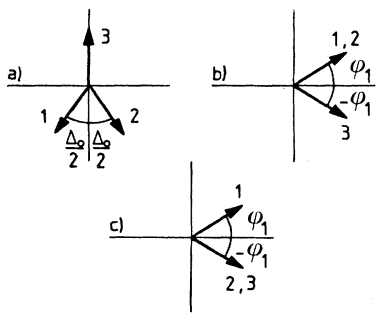

FIG. 9. Angular configuration at level $l = 0$ for some of the incommensurate homogeneous phases: (a) $(+ + +)_1$, (b) $(+ + -)_1$, and (c) $(- + +)_1$.

This is typical of partially frustrated antiferromagnetic triangular lattice and agrees with the result obtained by Tanaka and Kakurai [9] for the low-temperature phase when the exchange interaction between a displaced site and an undisplaced site is larger than between undisplaced sites. This is certainly our case since the displacement of the columns effectively doubles the number of first neighbor sites for the displaced molecules. In our case, the deviation from collinearity $\Delta_0/2$ is determined by the intracolumnar relative angle of neighboring molecules in the homogeneous helical state.

Finite value of the nonrotationally invariant term G and large enough values of $|J|$ pin the homogeneous phases into the uniform phase with $\Delta_0 = 0$. For this uniform phase, umklapp terms contribute and the angular configurations are frozen in different configurations with respect to the lattice in the limit of $J \to \pm\infty$. The transition from one angular configuration, for $J \to \infty$, to another configuration, for $J \to -\infty$, is achieved through two successive second-order transitions at large G (see Fig. 2).

For finite values of G, helically ordered phases with mixed helical pattern $(+\,+\,-)$ and $(-\,+\,+)$ are found. When redrawn in the $l = 0$ plane, the angular configuration for the phase $(+\,+\,-)_1$ is as shown in Fig. 9(b) and that of the phase $(-\,+\,+)_1$ is as in Fig. 9(c).

The study of the nonhomogeneous phases reveals the major role played by umklapp terms in these systems. Indeed, in Sec. IV it was shown that commensurate phases with finite winding number p/q occupy a very large fraction of the phase diagram. It may even be argued that for systems of infinite size, the incommensurate phases could be reduced to a phase space of measure zero. However, due to the limitations of finite-size systems, this is a question for which there is no definite answer in the present calculation.

In Fig. 5 four points are shown explicitly where the first-order transition boundaries between the 1/4 and the 0/1 phase terminate. They are also the convergence points of an infinite number of phases with winding number $p/q < 1/4$. This points to the fact that for the choice of parameters, the 1/4 phase stands as that phase with the largest pitch that occupies a fully connected region of the phase diagram. This can be understood, in general terms, by the balance between the J and G terms, which together force the angular configurations to be $\phi_{il} = 0$ or π and the intracolumnar term that gives $\phi_{il+1} - \phi_{il} = \Delta$. Let us follow the line $J = G$ for the $(+\,+\,-)$ phase to facilitate the interpretation of the nonhomogeneous phase diagram. The energy (8) is then given by

$$E = -J\sum_l \cos(\phi_{1l})\cos(\phi_{2l}) - J\sum_l\sum_{i=1}^{2}[\cos(\phi_{il})\cos(\phi_{3l}) + \cos(\phi_{il+1})\cos(\phi_{3l})] - \sum_l\sum_{i=1}^{3}\cos(\phi_{il+1} - \phi_{il} - \Delta) \quad (29)$$

and the angular configuration of pitches $1/q$ for $q \geq 4$ are similar to those of Fig. 7.

For phases of pitch $3/8 \leq p/q \leq 1/4$, the system is able to accommodate every term in (29). This compromise permits the gradual unwinding of the helix in a devil's staircase. As far as can be calculated with a finite system, these phases are stabilized over a fully connected region spanning over positive and negative J.

The pitch of the last fully connected phase to be stabilized, 1/4 in our case, is certainly a function of Δ solely. In fact, Δ leaves a signature on the angular configuration of the 1/4 phase (top panel in Fig. 7). In conjuction with (29), we can see that when the J and G terms cannot lower the energy ($\phi_{11} = \phi_{21} = \theta$, and $\phi_{12} = \phi_{22} = \pi - \theta$), the system discards these contributions (using $\phi_{31} = \frac{\pi}{2}$) to lower the intrachain energy $[\phi_{12} - \phi_{11} - \Delta = \pi - (2\theta + \Delta) \simeq 0]$.

The angular configuration of the 1/5 phase along the $J = G$ line, near the boundary between the 1/4 and 0/1 phases, is represented in the second panel of Fig. 7. This configuration slightly lowers the energy via the J and G terms, but greatly increases the intrachain interaction energy, adding up to a global increase in energy. In subsequent additions of spins along the x axis (portions of the 0/1 phase to generate phases 1/6, 1/7, 1/8, etc.) this global increase in energy is reduced, thus favoring the direct passage from the 1/4 phase to the uniform 0/1 phase. This explanation can be extended to $J \neq G$ and J positive and negative.

Finally, let us return to the physical system studied: HHTT columnar liquid crystal in the low-temperature phase. As indicated in Sec. I, the intracolumnar turn angle between adjacent molecules has been reported as $\alpha = 45°$ ($\Delta = 135°$). The phase diagram in Figs. 5 and 6 has been calculated with this value. Two observations can be made. First, the 3/8 phase is stable over a minute portion of the J-G phase diagram for the three columns. This leads us to conclude that a self-consistent field stabilizes the 3/8 phase even for the displaced column. This is not what was predicted for non-self-consistent field [11], but is in agreement with published experimental data [2–4]. Second, the helicity configurations are not the one observed experimentally [the $(+\,+\,-)$ phase]. Only the $(+\,+\,+)$ and $(-\,+\,+)$ helicity configurations of the 3/8 phase are reported. However, this can be overcome by making α slightly less than 45°, which is certainly admissible from the basic molecular calculations [21], in order to have the intermolecular intracolumnar interaction parameters stabilize the 3/8 phase in the $(+\,+\,-)$ region of the phase diagram.

In conclusion, we have clearly shown from the study of a simple but realistic three-dimensional model that the helical pattern $(+\,+\,-)$, where the displaced columns have opposite helicity to the undisplaced columns, results from the nonrotationally invariant terms in the Hamiltonian. Furthermore, the mechanism by which the system is driven in a particular commensurate phase under the action of the intercolumnar interactions is demonstrated. Finally, the study of the full phase diagram reveals a rich situation justifying a systematic experimental approach, in particular by taking advantage of the great diversity offered by material synthesis for these columnar liquid crystal systems.

ACKNOWLEDGMENTS

We thank M.L. Plumer for useful discussions. This work was supported by the National Sciences and Engineering Research Council of Canada, the Fonds pour la Formation des Chercheurs et de l'Aide à la Recherche du Québec, and the Centre de Recherche en Physique du Solide of the Université de Sherbrooke.

[1] We adopt the terminology proposed by P. G. de Gennes and J. Prost, *The Physics of Liquid Crystals* (Ref. [6]).
[2] E. Fontes, P.A. Heiney, and W.H. de Jeu, Phys. Rev. Lett. **61**, 1202 (1988).
[3] P.A. Heiney, E. Fontes, W.H. de Jeu, A. Reira, P. Carroll, and A.B. Smith III, J. Phys. (Paris) **50**, 461 (1989).
[4] E. Fontes, Doctoral dissertation, University of Pennsylvania, 1989 (unpublished).
[5] S.H. Idziak, Doctoral dissertation, University of Pennsylvania, 1992 (unpublished).
[6] P.G. de Gennes and J. Prost, *The Physics of Liquid Crystals*, 2nd ed. (Oxford University Press, New York, 1993).
[7] A. Caillé and M. Hébert (unpublished).
[8] K. Adachi, K. Tadeka, F. Matsubara, M. Mekata, and T. Haseda, J. Phys. Soc. Jpn. **52**, 2202 (1983); M.L. Plumer, A. Caillé, and H. Kawamura, Phys. Rev. B **44**, 4461 (1991).
[9] H. Tanaka and K. Kakurai, J. Phys. Soc. Jpn. **63**, 3412 (1994).
[10] M. Hébert, A. Caillé, and A. BelMoufid, Phys. Rev. B **48**, 3074 (1993).
[11] A. Caillé, M. Hébert, and M.L. Plumer, Phys. Rev. B **49**, 3104 (1994).
[12] M.L. Plumer, A. Caillé, and O. Heinonen, Phys. Rev. B **47**, 8479 (1993).
[13] H.Y. Choi, A.B. Harris, and E.J. Mele, Phys. Rev. B **40**, 3766 (1989).
[14] D.H. Lee, J.D. Joannopoulos, J.W. Negele, and D.P. Landau, Phys. Rev. B **33**, 450 (1986).
[15] M. Hébert and A. Caillé, Phys. Rev. E **51**, R1651 (1995).
[16] R.B. Griffiths and W. Chou, Phys. Rev. Lett. **56**, 1929 (1986); W. Chou and R.B. Griffiths, Phys. Rev. B **34**, 6219 (1986); F. Seno, J.M. Yeomans, R. Harbord, and D.Y.K. Ko, *ibid.* **49**, 6412 (1994).
[17] M. Marchand, K. Hood, and A. Caillé, Phys. Rev. Lett. **58**, 1660 (1987).
[18] H.T. Diep, A. Ghazali, and P. Lallemand, J. Phys. C **18**, 5881 (1985).
[19] C.S.O Yokoi, L.H. Tang, and W. Chou, Phys. Rev. B **37**, 2173 (1988).
[20] M.L. Plumer, A. Caillé, A. Mailhot, and H.T. Diep, in *Magnetic Systems with Competing Interactions (Frustrated Spin Systems)*, edited by H.T. Diep (World Scientific, Singapore, 1994).
[21] M. Pesquer, M. Cotrait, P. Marsau, and V. Volpilhac, J. Phys. (Paris) **41**, 1039 (1980).